Nucleon distribution in nuclei beyond β-stability line

V.M. Kolomietz, S.V. Lukyanov and A.I. Sanzhur

Abstract

The radii of nucleon distribution, bulk density, and neutron skin in nuclei beyond the β-stability line are studied within the direct variational method. We evaluate the partial equation of state of finite nuclei and demonstrate that the bulk density decreases beyond the beta stability line. We show that the growth of the neutron skin in unstable nuclei does not obey the saturation condition because of the polarization effect. The value of the neutron-skin thickness $\Delta r_{np} = \sqrt{\langle r_n^2 \rangle} - \sqrt{\langle r_p^2 \rangle}$ is caused by the different radii (skin effect) and only slightly by the different shapes (halo effect) of neutron and proton distributions. The relative contribution of both effects depends on the competition between the symmetry energy, and the spin-orbit and Coulomb interactions. The calculations of the isovector shift of the nuclear radius Δr_{np} show its primarily linear dependence on the asymmetry parameter $X = (N - Z)/A$.

PACS numbers: 24.10.Cn, 21.60.Ev, 24.10.Nz, 24.30.Cz, 24.75+i

I. INTRODUCTION

Our knowledge about the properties of neutron excess in heavy nuclei and its relation to the neutron-rich nuclear matter and the isotopic symmetry energy is still strongly limited. In heavy stable nuclei, the average changes in binding energy E and nuclear radius R with nucleon content obey the saturation properties. The volume part $E_{\rm vol}$ of binding energy and the nuclear volume itself are proportional to the particle number A with $E_{\rm vol} = -\, b_V A$ and $R = r_0 A^{1/3}$, where $b_V > 0$ and r_0 are the constants. Both values of b_V and r_0 depend, however, on the isotopic asymmetry parameter $X = (N - Z)/(N + Z)$. This is because of the difference in saturation bulk density, $\rho_0 \sim r_0^{-3}$, of nuclei with different values of X. The saturation density ρ_0 is smaller beyond the beta-stability line for neutron-rich nuclei where more neutrons are pushed off to form the "neutron coating". One can expect then that the growth of the neutron skin in neutron-rich nuclei violates the saturation property $R \sim A^{1/3}$ for the nuclear radius providing a relative shift of both neutron and proton distributions [1]. The main characteristic of the neutron skin is the neutron-skin thickness $\Delta r_{np} = \sqrt{\langle r_n^2 \rangle} - \sqrt{\langle r_p^2 \rangle}$, where $\sqrt{\langle r_n^2 \rangle}$ and $\sqrt{\langle r_p^2 \rangle}$ are the neutron and proton root mean square (rms) radii , respectively. The value of Δr_{np} can be caused by the different radii (skin effect) and the different shapes (halo effect) of neutron and proton distributions; see also Refs. [2–6]. The relative contribution of both effects depends on the competition between symmetry energy, spin-orbit and Coulomb interactions [7, 8].

In the present paper we study a deviation of nucleon distribution from the saturation behavior in neutron-rich nuclei. We consider the influence of the spin-orbit and Coulomb forces on the neutron, $\sqrt{\langle r_n^2 \rangle}$, and proton, $\sqrt{\langle r_p^2 \rangle}$, rms radii as well as the relation of the shift Δr_{np} to the surface symmetry energy. We study also the related problems of the nucleon redistribution within the surface region (nuclear periphery), in particular, the neutron coating and the neutron excess for the nuclei far away from the β-stability line.

We combine the extended Thomas-Fermi (ETF) approximation which takes into consideration the corrections up to the order of $\hbar^2$ and the direct variational method assuming that the proton and neutron distributions are sharp enough, i.e., that the corresponding densities $\rho_p(\mathbf{r})$ and $\rho_n(\mathbf{r})$ fall from their bulk values to zero in a thin region around the surface. In our consideration, the thin-skinned densities $\rho_p(\mathbf{r})$ and $\rho_n(\mathbf{r})$ are generated by the profile functions which are eliminated by the requirement that the energy of the nucleus should

be stationary with respect to variations of these profiles. Note that the use of the direct variational method and the trial profile function for the particle density allows us to derive the equation of state (the dependence of the pressure on the bulk density) in the case of the finite diffuse layer of the particle distribution in finite nuclei.

This paper is organized as follows. In Sec. II we formulate the direct variational principle for the density profile function within the extended Thomas-Fermi approximation. Using the leptodermous assumption, we obtain $A^{1/3}$ expansion for the symmetry energy and the related values. The results of numerical calculations are presented in Sec. III. We conclude and summarize in Sec. IV.

II. DIRECT VARIATIONAL APPROACH

We will use the extended Thomas-Fermi approximation which is one of the practical realizations of the general Hohenberg-Kohn theorem [9] on the unique functional relation between the ground-state energy and the local density of particles for any fermion system. The key point of the ETF is that the total kinetic energy of the many-body fermion system is given by the semiclassical expression [10–12] as follows:

$$E_{\rm kin}\{\rho_n,\rho_p\} \equiv E_{\rm kin}\{\rho_q,\nabla\rho_q\} = \int d\mathbf{r}\ \epsilon_{\rm kin}[\rho_n(\mathbf{r}),\rho_p(\mathbf{r})], \tag{1}$$

where $\epsilon_{\rm kin}[\rho_n,\rho_p] = \epsilon_{{\rm kin},n}[\rho_n] + \epsilon_{{\rm kin},p}[\rho_p]$, and

$$\epsilon_{{\rm kin},q}[\rho_q] = \frac{\hbar^2}{2m}\left[\frac{3}{5}\,(3\,\pi^2)^{2/3}\,\rho_q^{5/3} + \beta\frac{(\nabla\rho_q)^2}{\rho_q} + \frac{1}{3}\,\nabla^2\rho_q\right]. \tag{2}$$

Here ρ_q is the nucleon density with $q = n$ for neutron and $q = p$ for proton. The semiclassical consideration gives the value of parameter β in Eq. (2) $\beta = 1/36$ [10, 11]. We point out that in the asymptotic limit $r \to \infty$, the semiclassical particle density ρ_q with $\beta = 1/36$ goes significantly faster to zero than the one from the quantum-mechanical calculation. An asymptotic solution for the particle density $\rho_{{\rm ETF},q}(\mathbf{r})$ within the semiclassical extended Thomas-Fermi approximation in the limit $r \to \infty$ has the following form [11]:

$$\rho_{{\rm ETF},q}(\mathbf{r})|_{r\to\infty} \sim \frac{1}{r^2}\,\exp\left[-\sqrt{-\frac{2m}{\hbar^2}\,\frac{\lambda_q}{\beta}}\,r\right], \tag{3}$$

where λ_q is the chemical potential which is negative for a bound Fermi system. A quantum-mechanical wave function whose bound s orbital has energy ϵ, gives the partial contribution to the asymptotic particle density, which is

$$\rho_{\rm part}(\mathbf{r})|_{r\to\infty} \sim \frac{1}{r^2}\,\exp\left[-2\,\sqrt{-\frac{2\,m}{\hbar^2}\,\epsilon}\,r\right]. \tag{4}$$

Thus, the semiclassical particle density $\rho_{{\rm ETF},q}(\mathbf{r})$ of Eq. (3) for $\beta = 1/36$ goes faster to zero than the quantum-mechanical one (4). To overcome this defect of the extended Thomas-Fermi approximation the value β can be considered as an adjustable parameter. We will apply both the semiclassical value $\beta = 1/36$ and the phenomenological one $\beta = 1/9$ which is consistent with the quantum-mechanical asymptotic behavior given by Eq. (4).

We will follow the concept of the effective nucleon-nucleon interaction using the Skyrme-type force. The functional of the total energy of charged nucleus is given by

$$E_{\rm tot}\{\rho_q, \nabla\rho_q\} = E_{\rm kin}\{\rho_q, \nabla\rho_q\} + E_{\rm pot}\{\rho_q, \nabla\rho_q\} + E_{\rm C}\{\rho_p\}, \tag{5}$$

where $E_{\rm pot}\{\rho_q, \nabla\rho_q\}$ is the potential energy of NN interaction

$$E_{\rm pot}\{\rho_q, \nabla\rho_q\} = \int d\mathbf{r}\;\epsilon_{\rm pot}[\rho_n(\mathbf{r}), \rho_p(\mathbf{r})], \tag{6}$$

$\epsilon_{\rm pot}[\rho_n(\mathbf{r}), \rho_p(\mathbf{r})]$ is the density of the potential energy of the nucleon-nucleon interaction and $E_{\rm C}\{\rho_p\}$ is the Coulomb energy. In our consideration, the potential energy $E_{\rm pot}\{\rho_q, \nabla\rho_q\}$ includes the energy of the spin-orbit interaction also.

Following the direct variational method, we have to choose the trial function for $\rho_q(\mathbf{r})$. We will assume a power of the Fermi function for $\rho_q(\mathbf{r})$ as

$$\rho_q(\mathbf{r}) = \rho_{0,q}\left[1 + \exp\left(\frac{r - R_q}{a_q}\right)\right]^{-\eta}, \tag{7}$$

where $\rho_{0,q}$, R_q, a_q, and η are the unknown variational parameters. Considering the asymmetric nuclei with $X = (N - Z)/A \ll 1$, we will introduce the isotopic particle densities, namely the total density $\rho_+ = \rho_n + \rho_p$ and the neutron excess density $\rho_- = \rho_n - \rho_p$ with $\rho_- \ll \rho_+$. Assuming a small deviation of the isoscalar bulk density $\rho_{0,+} = \rho_{0,n} + \rho_{0,p}$, the radii R_q, and the diffuseness parameters a_q with respect to the corresponding average values of ρ_0, R, and a, we introduce the density profile functions $\rho_+(r)$ and $\rho_-(r)$ to be given by

$$\rho_+(r) = \rho_0\, f(r) - \frac{1}{2}\rho_1 \frac{df(r)}{dr}\left[\Delta_R + \frac{r-R}{a}\Delta_a\right], \quad \rho_-(r) = \rho_1\, f(r) - \frac{1}{2}\rho_0 \frac{df(r)}{dr}\left[\Delta_R + \frac{r-R}{a}\Delta_a\right]. \tag{8}$$

Here,

$$f(r) = \left[1 + \exp\left(\frac{r-R}{a}\right)\right]^{-\eta}, \tag{9}$$

the values ρ_0 and ρ_1 are related to the bulk density, R is the nuclear radius, a is the diffuseness parameter, and $\Delta_R = R_n - R_p$ and $\Delta_a = a_n - a_p$ are the parameters of the neutron skin. The profile functions $\rho_+(r)$ and $\rho_-(r)$ have to obey the condition that the number of neutrons and protons is conserved. For the ground state of the nucleus, the unknown parameters ρ_0, ρ_1, R, a, Δ_R, Δ_a, and η and the total energy $E_{\rm tot}$ itself can be derived from the variational principle

$$\delta(E - \lambda_n N - \lambda_p Z) = 0, \tag{10}$$

where the variation with respect to all possible small changes of ρ_0, ρ_1, R, a, Δ_R, Δ_a, and η is assumed. The Lagrange multipliers λ_n and λ_p are the chemical potentials of the neutrons and the protons, respectively, and both of them are fixed by the condition that the number of particles is conserved.

We point out that the bare nucleon mass m, but not the effective one m^*, enters the kinetic energy density $\epsilon_{{\rm kin},q}[\rho_q]$ in Eq. (2) and accompanies the direct variational procedure of Eq. (10). This is due to the fact that the expression (2) is directly obtained as a result of a Wigner transform to the quantum-mechanical kinetic energy of many-body systems where only the bare mass m is available; see, e.g., Ref. [10]. Usually, the effective mass m^* appears in the self-consistent Euler equations for the particle density ρ_q within the Thomas-Fermi approach (or for the single-particle wave functions in the case of Hartree-Fock theory) after the implementation of the corresponding variational procedure. The effective mass appears there because the part of the self-consistent mean field, which is caused by the non-local interparticle interaction, is associated with the single-particle kinetic energy. In contrast, in our direct variational method we do not use the Euler equations for the particle density. Thereby, the effective mass m^* cannot be included in the kinetic energy density $\epsilon_{{\rm kin},q}[\rho_q]$ of Eq. (2) to avoid a twofold account of contributions from the t_1- and t_2- components of Skyrme forces which enter already the potential energy density $\epsilon_{\rm pot}[\rho_q(r)]$ in Eq. (6). This argument is also applied to the spin-orbit interaction in a finite system where the spin-orbit

contribution to the energy functional $E_{\rm pot}\{\rho_q, \nabla\rho_q\}$ of Eq. (6) is involved in the direct variational procedure as well.

We will also assume that the leptodermous condition $a/R \ll 1$ is fulfilled. The total energy (equation of state) (5) takes then the following form [13]:

$$E_{\rm tot}(\rho_0, X)/A = e_0(\rho_0) \ + b_{\rm S}(\rho_0)A^{-1/3} + \left[b_{\rm V,sym}(\rho_0) + b_{\rm S,sym}(\rho_0)\ A^{-1/3}\right] X^2 + E_C(\rho_0, X)/A, \tag{11}$$

where $e_0(\rho_0)$ is the energy per nucleon of symmetric nuclear matter, $b_{\rm S}(\rho_0)$ is the surface energy coefficient, $b_{\rm V,sym}(\rho_0)$ is the volume part of symmetry energy coefficient, $b_{\rm S,sym}(\rho_0)$ is the surface part of the symmetry energy coefficient, and $E_C(\rho_0, X)$ is the total Coulomb energy

$$E_C(\rho_0, X) = \alpha_C(\rho_0)\,(1-X)^2\,A^{5/3} + O(A^{4/3}), \quad \alpha_C(\rho_0) = \frac{3}{20}e^2\left(\frac{4\pi\rho_0}{3}\right)^{1/3}. \tag{12}$$

The equation of state in the form of Eq. (11) implies that the total energy per particle $E_{\rm tot}(\rho_0, X)/A$ is minimized with respect to the independent parameters a, Δ_R, Δ_a, and η for arbitrary values of ρ_0 and X.

The structure of the equation of state (EOS) given by Eq. (11) is similar to the semiempirical mass formula which describes the average changes in nuclear binding energy with the mass number. However, in contrast to the mass formula, the bulk density ρ_0 and the asymmetry parameter are not necessarily at equilibrium. The symmetry term $\sim X^2$ includes both the volume, $b_{\rm V,sym}(\rho_0)$, and the surface, $b_{\rm S,sym}(\rho_0)$, contributions. The surface symmetry term $b_{\rm S,sym}(\rho_0)\ A^{-1/3}X^2$ appears in the advanced mass formula by Myers and Swiatecki [14, 15] and it is currently employed in the description of surface properties and isovector excitations in finite nuclei; see, e.g., Refs. [16, 17].

For a given bulk density ρ_0, one can derive the beta-stability line $X = X^*(A, \rho_0)$ by the condition

$$\left.\frac{\partial E_{\rm tot}(\rho_0, X)/A}{\partial X}\right|_{A,\ X=X^*} = 0. \tag{13}$$

Near the beta-stability line, the total energy per particle (11) is written up to the order $(X - X^*)^2$ as

$$E_{\rm tot}(\rho_0, X)/A = E_{\rm tot}(\rho_0, X^*)/A + \left[b_{\rm V,sym}(\rho_0) + b_{\rm S,sym}(\rho_0)\ A^{-1/3} - \alpha_C(\rho_0)A^{2/3}\right](X - X^*)^2. \tag{14}$$

[Note that Eq. (14) is written for $A =$ constant.] The energy of the ground state for a given value of mass number A is obtained from the additional equilibrium condition

$$\frac{\partial}{\partial \rho_0} E_{\rm tot}(\rho_0, X^*)/A \Big|_{A,\rho_0=\rho_{0,\rm eq}} = 0, \tag{15}$$

where $\rho_{0,\rm eq}$ is the equilibrium bulk density.

The parameters Δ_R and Δ_a in the profile functions of Eq. (8) derive the neutron skin, Δr_{np}, and the neutron excess, N_S, in the surface region of the nucleus ("neutron coating"). Substituting Eqs. (8) and (9) into the conservation particle condition and using the leptodermous expansion, we obtain for the neutron excess $N - Z$ the following expression

$$N - Z \approx N_V + N_S, \tag{16}$$

where

$$N_V \approx \frac{4\pi}{3} R^3 \left(1 + 3\kappa_0(\eta)\frac{a}{R} + 6\kappa_1(\eta)\left(\frac{a}{R}\right)^2\right)\rho_1, \tag{17}$$

$$\begin{aligned} N_S \approx 4\pi R^2 \Bigg[\Delta_R \left(1 + 2\kappa_0(\eta)\frac{a}{R} + 2\kappa_1(\eta)\left(\frac{a}{R}\right)^2\right) \\ + \Delta_a \left(\kappa_0(\eta) + 4\kappa_1(\eta)\frac{a}{R} + 3\kappa_2(\eta)\left(\frac{a}{R}\right)^2\right)\Bigg]\frac{\rho_0}{2}, \end{aligned} \tag{18}$$

where $\kappa_j(\eta)$ are the generalized Fermi integrals derived in Ref. [13]

$$\kappa_j(\eta) = \int_0^\infty dx\, x^j \left[(1+e^x)^{-\eta} - (-1)^j \left(1 - (1+e^{-x})^{-\eta}\right)\right]. \tag{19}$$

The first term $N_V \sim R^3$ on the right hand side of Eq. (16) is caused by the redistribution of the neutron excess within the nuclear volume while the second one $N_S \sim R^2$ is the neutron coating.

Note that the variational conditions of Eq. (10) leads to an additional dependence of the variational parameters ρ_0, ρ_1, R, a, Δ_R, Δ_a and η on the external parameters A and X. The values of Δ_R and Δ_a depends slightly on the Skyrme force parametrization. In the case of the SkM forces we have evaluated the dependence of Δ_R and Δ_a on X for $A = 120$ numerically and fitted it by the following formula

$$\Delta_R(X) \approx 1.34\ X + 0.07\ X^2 \text{ fm}, \quad \Delta_a(X) \approx 0.36\ X + \ 0.53\ X^2 \text{ fm}. \tag{20}$$

In general, the change of the radius R of the nucleon distribution with the nucleon number A is caused by two factors. There is a simple geometrical change of R because of

$R \propto A^{1/3}$. An additional change can occur due to the polarization effect (the bulk density distortion) with moving away the beta-stability line. In particular, the size of the neutron skin is sensitive to the symmetry and Coulomb energies. To see that we expand the total energy $E_{\rm tot}(\rho_0, X)/A$ around the saturation density $\rho_{0,\rm eq}$. By keeping only terms quadratic in $\delta\rho_0 = \rho_0 - \rho_{0,\rm eq}$ we rewrite equilibrium Eq. (14) as [18]

$$E_{\rm tot}(\rho_0, X)/A = E_{\rm tot}(\rho_{0,\rm eq}, X^*)/A + \frac{K_A}{18\rho_{0,\rm eq}^2}(\rho_0 - \rho_{0,\rm eq})^2 + \frac{P_{A,\rm sym}}{\rho_{0,\rm eq}^2}(X - X^*)^2(\rho_0 - \rho_{0,\rm eq}), \quad (21)$$

where K_A is the incompressibility of finite nucleus

$$K_A = 9\ \rho_{0,\rm eq}^2 \frac{\partial^2 E_{\rm tot}(\rho_0, X^*)/A}{\partial \rho_0^2}\bigg|_{A,\rho_0=\rho_{0,\rm eq}} \quad (22)$$

and $P_{A,\rm sym}$ is the partial pressure related to the symmetry and Coulomb energies

$$P_{A,\rm sym} = \rho_{\rho_{0,\rm eq}}^2\ \frac{\partial}{\partial \rho_0}\left[b_{\rm V,sym}(\rho_0) + b_{\rm S,sym}(\rho_0)\ A^{-1/3} - \alpha_C(\rho_0) A^{2/3}\right]\bigg|_{A,\rho_0=\rho_{0,\rm eq}}. \quad (23)$$

As seen from Eq. (21), a deviation from the beta-stability line ($X \neq X^*$) implies the change of the bulk density ρ_0. The corresponding change of ρ_0 is dependent on the incompressibility K_A and the partial pressure $P_{A,\rm sym}$. For an arbitrary fixed value of X, the equilibrium density $\rho_{0,X}$ is derived by the condition

$$\frac{\partial}{\partial \rho_0} E_{\rm tot}(\rho_0, X)/A\bigg|_{A,\rho_0=\rho_{0,X}} = 0. \quad (24)$$

Using Eqs. (21) and (24), we obtain the expression for the shift of the bulk density (polarization effect) in the neutron rich nuclei

$$\rho_{0,X} = \rho_{0,\rm eq} - 9\frac{P_{A,\rm sym}}{K_A}(X - X^*)^2. \quad (25)$$

In Fig. 1 we have plotted the partial pressure $P_{A,\rm sym}(\rho_0)$ versus the bulk density ρ_0 (partial equation of state) for the nucleus ^{120}Sn. The partial contributions to $P_{A,\rm sym}(\rho_0)$ from the symmetry volume $\sim \partial b_{\rm V,sym}(\rho_0)/\partial\rho_0$, the symmetry surface $\sim \partial b_{\rm S,sym}(\rho_0)/\partial\rho_0$, and the Coulomb $\sim \partial\alpha_C(\rho_0)/\partial\rho_0$ terms are also plotted in Fig. 1. The dashed vertical line shows the position $\rho_0/\rho_{0,\rm eq} = 0.62$ of the spinodal instability border where $K_A = 0$. On the left side of this line the nucleus is unstable with respect to the bulk density variations.

As seen from Fig. 1, the equilibrium partial pressure $P_{A,\rm sym}(\rho_{0,\rm eq})$ is positive and thereby $\rho_{0,X} < \rho_{0,\rm eq}$; see also Refs. [19, 20]. We point out that in general the sign of the equilibrium partial pressure $P_{A,\rm sym}(\rho_{0,\rm eq})$ depends on the Skyrme force parametrization and this fact can be used to fit the Skyrme forces [21].

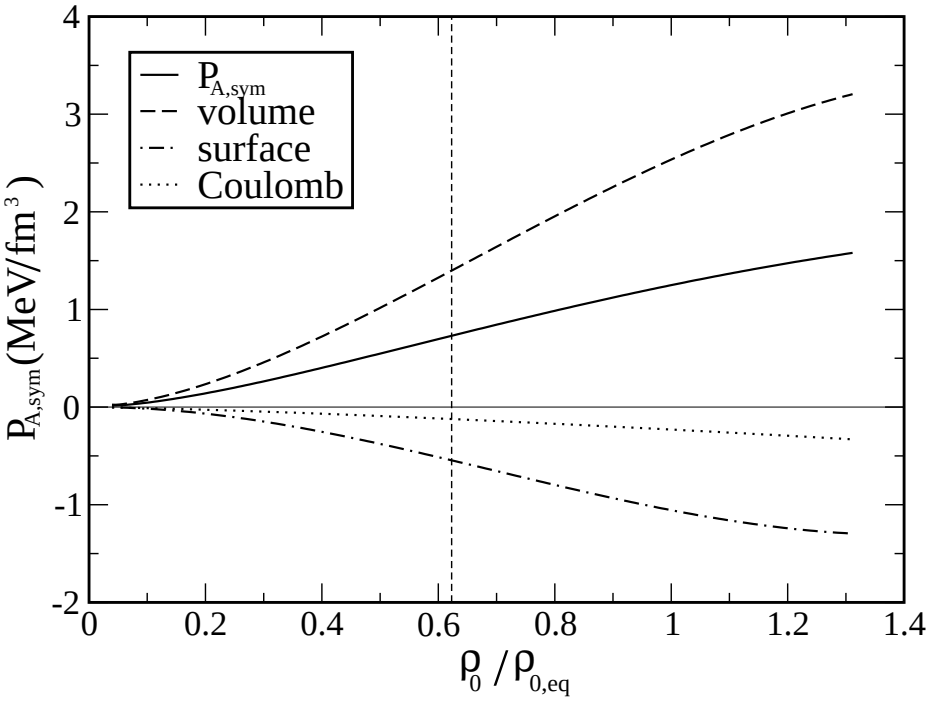

FIG. 1. The partial pressure $P_{A,\mathrm{sym}}$ for the nucleus ^{120}Sn calculated for the SkM parametrization of the Skyrme force. The equilibrium bulk density $\rho_{0,eq} \simeq 0.153$ fm^{-3}. The dashed vertical line is the spinodal instability border.

III. RADII OF NUCLEON DISTRIBUTIONS AND NEUTRON SKIN

As above noted, the bulk density $\rho_{0,X}$ is smaller for neutron-rich nuclei; more neutrons should be pushed off to enrich the skin providing a polarization effect. The nuclear rms radius

$$\sqrt{\langle r^2 \rangle} = \sqrt{\int d\mathbf{r}\, r^2\, \rho_+(r) / \int d\mathbf{r}\ \rho_+(r)}. \tag{26}$$

does not necessarily obey then the saturation condition having that $\sqrt{\langle r^2 \rangle}$ is nonproportional to $A^{1/3}$. As a consequence, the nuclei with significant excess of neutrons exhibit neutron coating, i.e., are characterized by larger radii for the neutron than for proton distributions. The interest in the neutron coating was recently raised because of expectations that an analysis of the neutron coating could permit extrapolating the nuclear properties to neutron matter [19]. From the point of view of study of the EOS, the coating size could provide information on the derivative of the symmetry energy with respect to the particle density [19, 22, 23]. In general, the neutron coating N_S of Eq. (17) can indicate the possibility of a

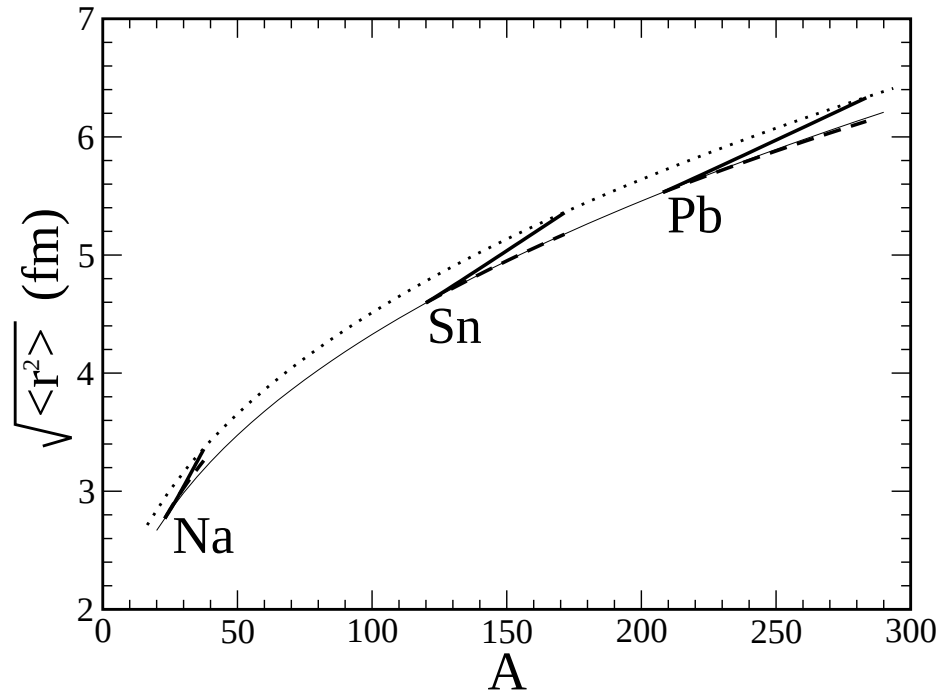

FIG. 2. The rms radius of nuclei near the beta-stability line. The thin solid line is for the beta-stability line, the thick solid line is beyond the beta-stability line for three nuclei, and the dotted curve is for the neutron drip line. The dashed lines are the rms radii calculated with the step distribution (27). The calculations have been performed for the SkM parametrization of the Skyrme force.

giant neutron halo which grows with moving away from the beta stability line [1].

In Fig. 2 we have plotted (see the thick solid lines) the nuclear rms radii $\sqrt{\langle r^2 \rangle}$ obtained from Eq. (26) for three nuclei. The results of Fig. 2 are only slightly sensitive to a small variation of the diffuse layer and we have here assumed that $\Delta_a = 0$. The thin solid line of Fig. 2 represents the rms radius $\sim A^{1/3}$ along the beta-stability line $X = X^*(A)$ which is parametrized by $X^*(A) = 0.17A^{2/3}\big/\big(26.5 - 25.6A^{-1/3} + 0.17A^{2/3}\big)$ [24]. The deviation of the rms radii (thick solid lines) from the saturation behavior $\sim A^{1/3}$ (thin solid line) can not be related directly to the appearance of the giant neutron halo at the approach to the drip line (dotted curve) because we have here assumed $\Delta_a = 0$. As above noted, there are two sources for the change of the radius of nucleon distribution with the nucleon number A. The first one is due to a simple geometrical reason and the second one is because of the polarization effect; see Eq. (25). To extract a simple geometrical change of the rms radius

$\sqrt{\langle r^2\rangle}$ we will perform the calculations of $\sqrt{\langle r^2\rangle}$ with a step nucleon distribution

$$\rho(r) = \rho_0 \Theta(r - R). \tag{27}$$

Then the geometric rms radius calculated with the step function is given by

$$\sqrt{\langle r^2\rangle}\Big|_{\rm geom} = \sqrt{\frac{3}{5}} R.$$

We will normalize the "geometrical" rms radius to the one $\sqrt{\langle r^2\rangle^*}\Big|_{\rm geom} = \sqrt{3/5}R^*$, where R^* is the nuclear radius on the beta-stability line which obeys the saturation behavior $R^* = r_0 A^{1/3}$. Finally we obtain

$$\sqrt{\langle r^2\rangle}\Big|_{\rm geom} = \sqrt{\frac{3}{5}} R^* \left(\frac{1 - X^*}{1 - X}\right)^{1/3}. \tag{28}$$

The results of calculations by use of Eq. (28) are shown in Fig. 2 with the dashed lines. As one can see these results for the nuclei ^{23}Na, ^{120}Sn, and ^{208}Pb are very close to the ones on the beta-stability line (thin solid line). The difference between the dashed lines and the thick solid ones represents the magnitude of the polarization effect given by Eq. (25). Thus, we can conclude that the deviation of $\sqrt{\langle r^2\rangle}$ from the saturation behavior $\sim A^{1/3}$ in the regions of medium and heavy nuclei is caused by the polarization effect which perturbs the distribution of the neutron excess.

To check the origin of the polarization effect, we have plotted in Fig. 3 the relative shift of the neutron and proton radii Δ_R/R and the diffuseness parameters Δ_a/a versus the neutron excess $N - Z$ for the fixed $Z = 50$. Note that the direct use of the variational procedure (10) with the modified profile functions $\rho_+(r)$ and $\rho_-(r)$ of Eq. (8) is badly converged with respect to the variations of the parameter Δ_a. To overcome this difficulty in Fig. 3, we have performed the variational calculations by use of the basic trial functions Eq. (7). One can see from Fig. 3 that the parameter $\Delta_a/a = (a_n - a_p)/a$, i.e., the parameter of the shape distribution, is appreciably growing with the growing of the neutron coating whereas the skin parameter Δ_R/R is only slightly sensitive to the increase of $N - Z$. We point out also that both shift parameters Δ_R and Δ_a are only slightly sensitive to the semiclassical gradient parameter β in Eq. (2).

The sensitivity of the rms radii of the nucleon distribution

$$\sqrt{\langle r_q^2\rangle} = \sqrt{\int d\mathbf{r}\, r^2\, \rho_q(r) / \int d\mathbf{r}\ \rho_q(r)}. \tag{29}$$

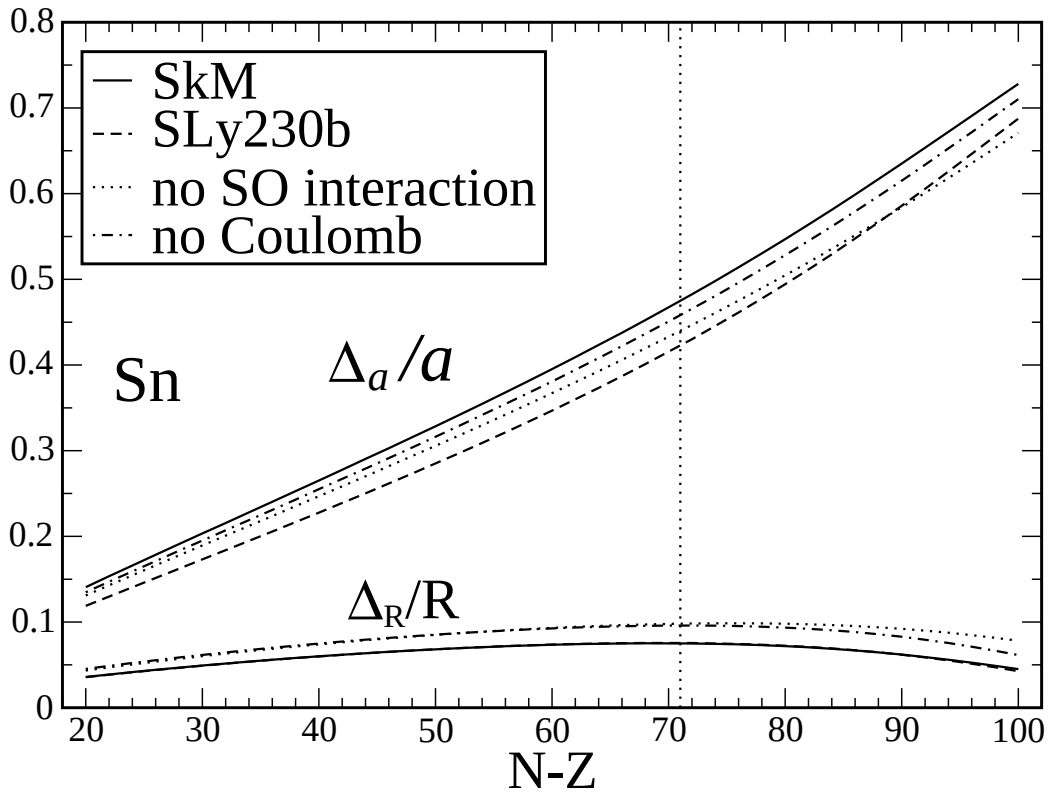

FIG. 3. Dependence of the relative shift of the neutron and proton radii $\Delta_R/R = (R_n - R_p)/R$ and the diffuseness parameters $\Delta_a/a = (a_n - a_p)/a$ versus the neutron excess $N-Z$ for the isotopes with $Z = 50$. The dotted line indicates no spin-orbit interaction and the dash-dotted line no Coulomb interaction for the SkM parametrization. The dashed line is for the SLy230b parametrization. The vertical dotted line is for the neutron drip line.

to the structure of the interparticle interaction is shown in Figs. 4 and 5 for Na isotopes. We can see from Fig. 4 that the ETFA results for $\sqrt{\langle r_n^2 \rangle}$ agree quite well with the experimental data from [25]. The sensitivity of the calculation of $\sqrt{\langle r_n^2 \rangle}$ to the choice of the Skyrme forces for two parametrizations, SkM and SLy230b, can also be seen. Such kind of sensitivity can be used to fit the Skyrme force parameters. The two additional lines in Fig. 4 show the influence of the spin-orbit and Coulomb interactions on $\sqrt{\langle r_n^2 \rangle}$. As was mentioned above, the spin-orbit interaction leads to the deeper potential in the surface region and therefore a nuclear core attracts external coating neutrons. This effect reduces the value of the polarization effect. The Coulomb interaction acts in the opposite direction. The last is because the Coulomb interaction increases the mean distance between nucleons and thereby the rms

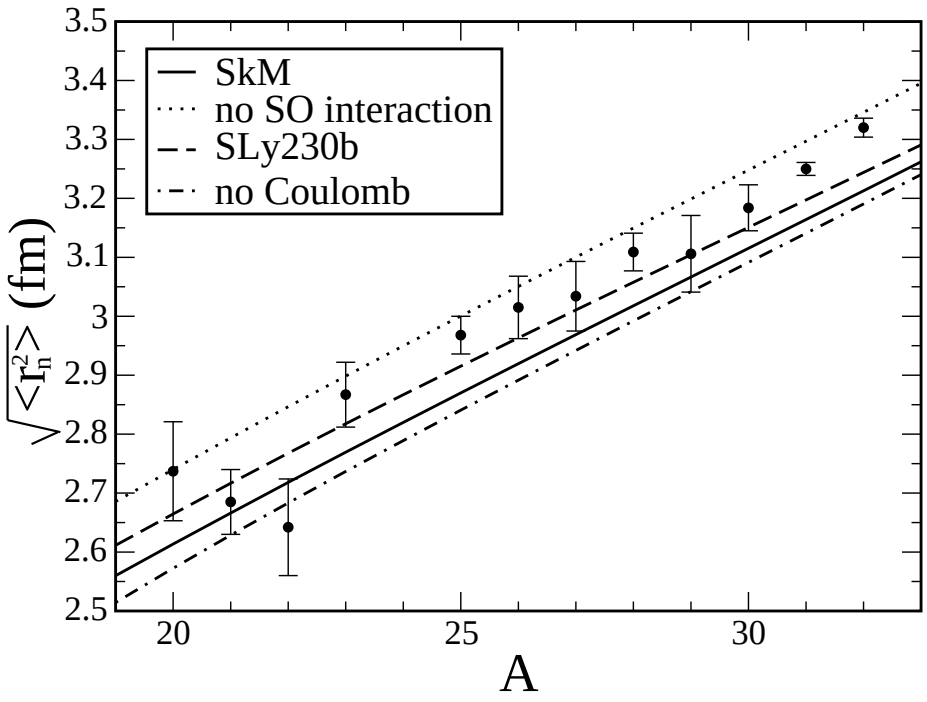

FIG. 4. The rms radius of neutron distribution in Na isotopes for the SkM parametrization (solid line). The dotted line indicates no spin-orbit interaction and the dash-dotted line no Coulomb interaction for the SkM parametrization. The dashed line is for the SLy230b parametrization.

radius.

The analogous results for the charge rms radius $\sqrt{\langle r_p^2 \rangle}$ of Na isotopes are shown in Fig. 5. A small increase of rms radius $\sqrt{\langle r_p^2 \rangle}$ of the proton distribution with an increase of the neutron number is caused by the neutron-proton attraction. Note that the experimental data for proton rms radius $\sqrt{\langle r_p^2 \rangle}$ in Fig. 5 manifests the non-monotonic behavior which is due to the shell effects. The influence of the spin-orbit and Coulomb interactions on the charge radius is the same as in the previously observed case for the rms neutron radius. Note also that such kind of behavior of $\sqrt{\langle r_p^2 \rangle}$ is correlated with the A dependence of the nuclear Coulomb radius R_C; see Ref. [18].

As mentioned in Sect. 1, the value of isotopic shift of radii Δr_{np} can be caused by both the skin effect and the halo effect in the neutron and proton distributions. To separate these effects, we will represent the value of Δr_{np} as

$$\Delta r_{np} = \Delta r_{np,R} + \Delta r_{np,a}, \tag{30}$$

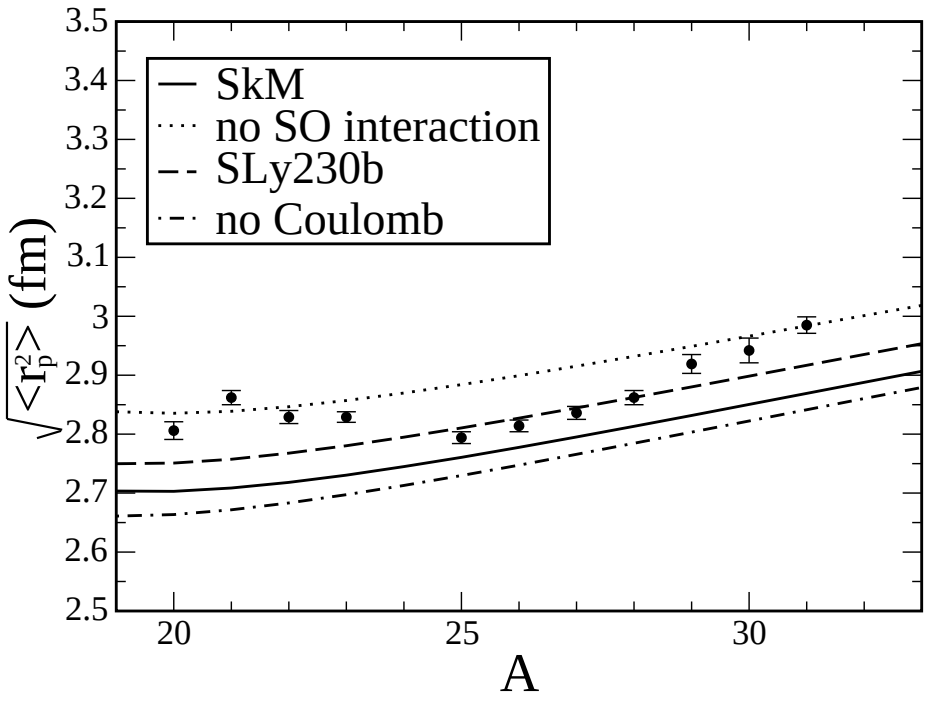

FIG. 5. The same as in Fig. 4 but for proton distribution.

where $\Delta r_{np,R}$ and $\Delta r_{np,a}$ are caused by the different radii (skin effect) and the different diffuseness (halo effect) of the neutron and proton distributions, respectively. The corresponding values are given by

$$\Delta r_{np,R} \approx \sqrt{\frac{3}{5}} \left\{ 1 + \frac{7}{2} \left[\kappa_0^2(\eta) - 2\kappa_1(\eta) \right] \left(\frac{a}{R} \right)^2 \right\} \Delta_R, \tag{31}$$

and

$$\Delta r_{np,a} \approx \sqrt{\frac{3}{5}} \left\{ \kappa_0(\eta) - 7 \left[\kappa_0^2(\eta) - 2\kappa_1(\eta) \right] \frac{a}{R} \right\} \Delta_a, \tag{32}$$

In Fig. 6 we have plotted the values of $\Delta r_{np,R}$ and $\Delta r_{np,a}$ versus the neutron excess for Sn isotopes.

As can be seen in Fig. 6, the relative contribution of the shape (halo) effect, i.e., $\Delta r_{np,a}$, to the isotopic shift of radii Δr_{np} depends strongly on the parameter β of the diffuse tail in the nucleon density distribution; see Eq. (3). For the semiclassical value of $\beta = 1/36$, the halo effect is quite small near the beta stability line and can play an appreciable role close to the drip line only. The situation is significantly different in the case of the phenomenological value of $\beta = 1/9$ where the contribution of $\Delta r_{np,a}$, and thereby the halo effect, to Δr_{np} is more appreciable.

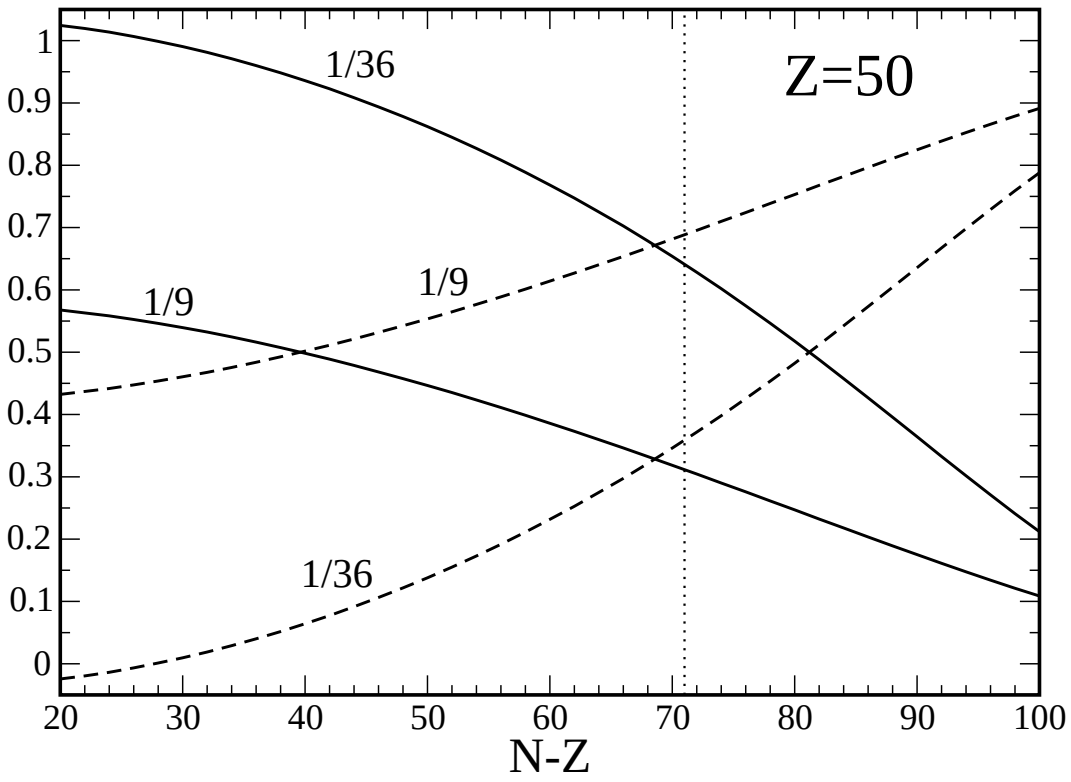

FIG. 6. The partial contribution to the isotopic shift of radii Δr_{np} from the skin effect, $\Delta r_{np,R}/\Delta r_{np}$ (solid lines), and the halo effect, $\Delta r_{np,a}/\Delta r_{np}$ (dashed lines), versus the neutron excess in Sn isotopes. The calculations have been performed for two values of the gradient parameter $\beta = 1/36$ and $\beta = 1/9$ indicated near the corresponding lines. The vertical dotted line is for the neutron drip line.

The A dependence of the size of the neutron coating $\Delta r_{np} = \sqrt{\langle r_n^2 \rangle} - \sqrt{\langle r_p^2 \rangle}$ is illustrated in Figs. 7, 8, and 9 for Na, Sn, and Pb isotopes, respectively. The numerical results have been obtained from Eq. (29) by use of the basic trial functions Eq. (7). The experimental data have been taken from Refs. [25–29].

As can be seen from Figs. 7, 8, and 9, the Coulomb interaction affects the isovector shift of nuclear radii weakly but with growing of A and X this influence slightly increases. The last is because the Coulomb interaction increases the distance between protons, i.e., $\langle r_p^2 \rangle$, and reduces thereby the isovector shift. The spin-orbit interaction produces the same effect as the Coulomb interaction but with stronger magnitude. As was mentioned above, the spin-orbit interaction leads to a deeper potential near the surface region and the nuclear

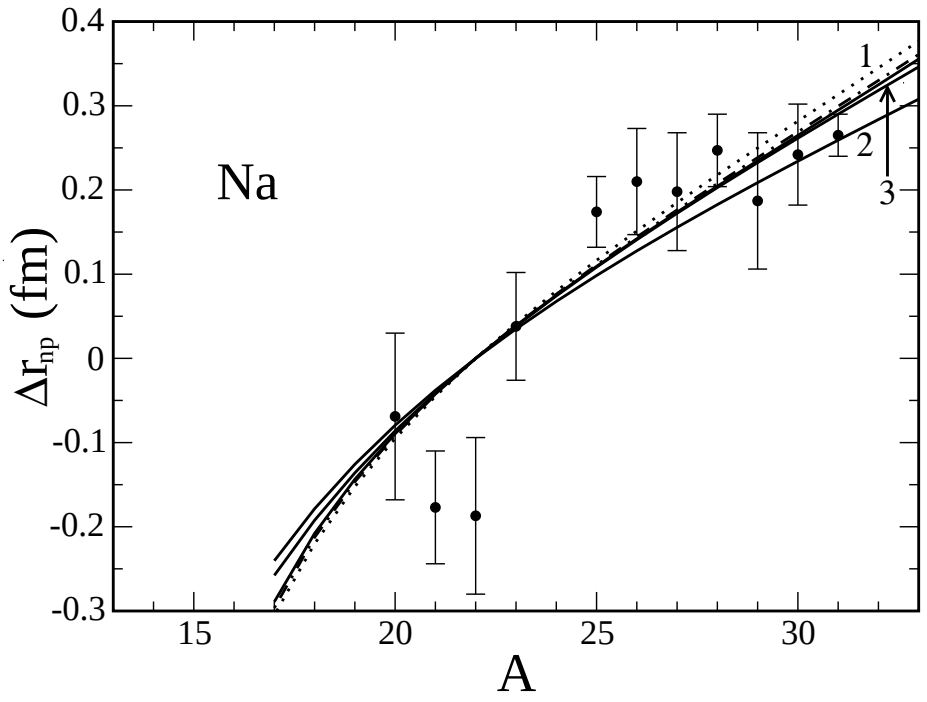

FIG. 7. Isovector shift of nuclear rms radius $\Delta r_{np} = \sqrt{\langle r_n^2 \rangle} - \sqrt{\langle r_p^2 \rangle}$ in Na isotopes for the SkM parametrization. Solid line 1 was obtained by use of trial functions Eq. (7), i.e., $\Delta_a \neq 0$, and $\beta = 1/36$. The dotted line is the same but without spin-orbit interaction and the dash-dotted line is without Coulomb interaction. The solid line 2 is for $\Delta_a = 0$ and $\beta = 1/36$; the solid line 3 is for $\Delta_a = 0$ and $\beta = 1/9$.

core attracts the external neutrons decreasing the diffuse layer of the neutron distribution. That reduces the isovector shift of nuclear radii because of Eqs. (30) and (32). The spin-orbit effect on Δr_{np} increases with X because the increase of X leads to the contribution to the density $\rho_n(r)$ of neutrons with higher angular momentum.

The value of the halo effect in Δr_{np} can be estimated from Figs. 7, 8, and 9 by comparison of the solid lines 1 and 2. The curve 2 was obtained neglecting the contribution from the isovector diffuseness distortion, i.e., for $\Delta_a = 0$. We can see that the halo effect, which occurs because of $\Delta_a \neq 0$, is quite small even for the lighter nucleus Na. As seen in Figs. 7, 8, and 9, the halo effect leads to an increase of the isovector shift Δr_{np} of nuclear radii. The change of the slope of curves $\Delta r_{np}(A)$ due to the halo effect can be also obtained analytically from Eqs. (30), (31), and (32). Taking into account a typical dependency of the values $\Delta_R(X)$ and $\Delta_a(X)$ on the asymmetry parameter X, see e.g. Eq. (20), and the fact that $\kappa_0(\eta) = -1$

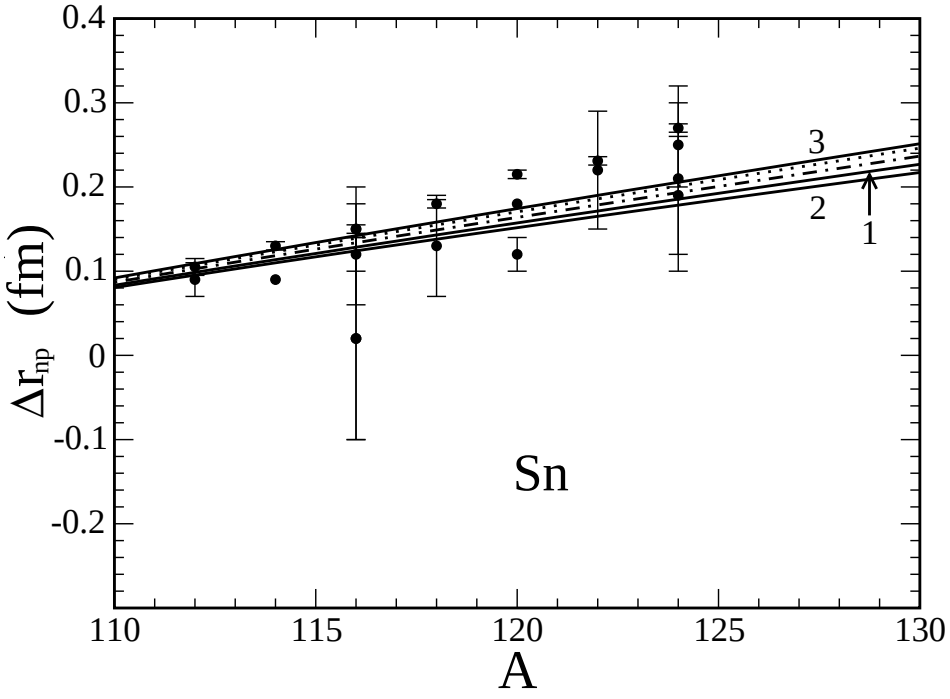

FIG. 8. The same as in Fig. 7 but for Sn isotopes.

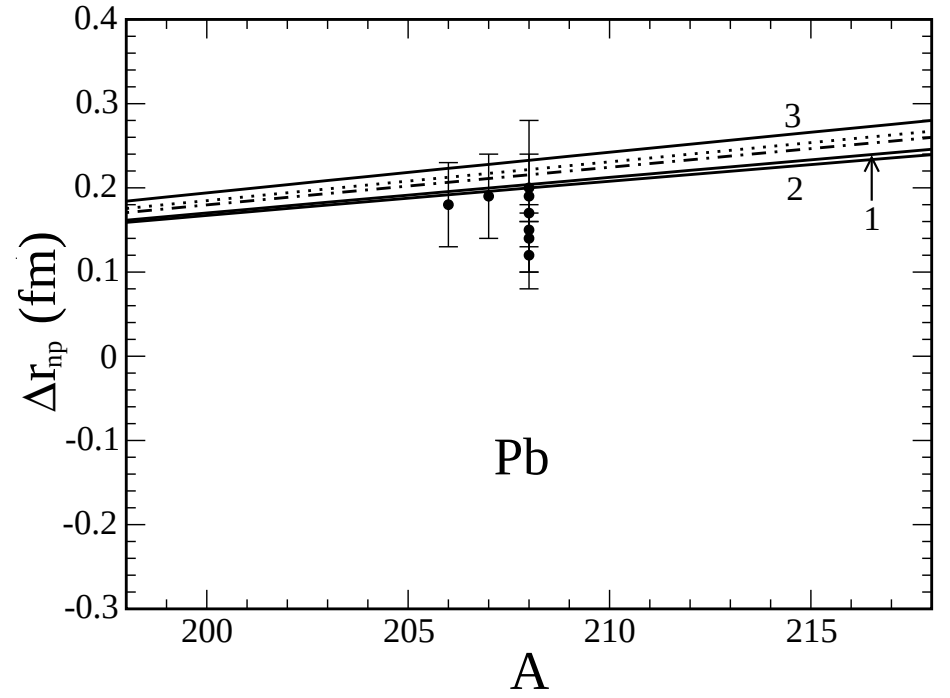

FIG. 9. The same as in Fig. 7 but for Pb isotopes.

and $\kappa_1(\eta) \simeq 1.65$ for $\eta = 2$, one can see that the slope of curves $\Delta r_{np}(A)$ grows with an increase of the diffuse layer shift Δ_a. Comparing the relative shifts of curves 1 and 2 in Figs. 7, 8, and 9, one can also conclude that the halo effect is reduced strongly for the heavier nuclei. This is because of a general increase of the nuclear stiffness with respect to the variation of the diffuse layer with growing A.

A growth of the parameter β which is responsible for the diffuse tail in the nucleon density distribution, see Eq. (3), increases the slope of the curve $\Delta r_{np}(A)$; see lines 2 and 3 in Figs. 7, 8, and 9. This is caused by the fact that the diffuse layer of the neutrons exceeds the one for the protons and the multiplication of the nucleon density $\rho_q(r)$ by a factor of r^2 in Eq. (29) leads to an emphasis of the peripheral region of the particle density which is stronger for the neutron peripheral region than for the proton one. Note also that the crossing point in Fig. 7 for isotopes of Na happens for $\Delta r_{np} = 0$ where $N = Z$.

IV. SUMMARY

We have applied the direct variational method within the extended Thomas-Fermi approximation with effective Skyrme-like forces to the description of the radii of nucleon distributions. In our consideration, the thin-skinned nucleon densities $\rho_p(\mathbf{r})$ and $\rho_n(\mathbf{r})$ are generated by the profile functions which are eliminated by the requirement that the energy of the nucleus should be stationary with respect to variations of these profiles. An advantage of the used direct variational method is the possibility to derive the equation of state for finite nuclei: dependence of the binding energy per particle or the pressure on the bulk density ρ_0. We have evaluated the partial pressure $P_{A,\mathrm{sym}}$ which includes the contributions from the symmetry and Coulomb energies. The pressure $P_{A,\mathrm{sym}}$ is positive driving off the neutrons in neutron-rich nuclei to the skin.

Using the leptodermous properties of the profile nucleon densities $\rho_p(\mathbf{r})$ and $\rho_n(\mathbf{r})$, we have established the presence of the neutron coating N_S. The size of the neutron coating is growing with moving away from the beta stability line. In Fig. 2 this fact is demonstrated as a deviation of the rms radius of the nucleon distribution from the saturation behavior $\sim A^{1/3}$ in the nuclei beyond the beta-stability line. Moreover, the neutron skin develops by diffusing the neutron surface against the changeless proton diffuseness and can be responsible for the giant neutron halo in neutron-rich nuclei.

The average behavior of the nucleon distribution $\sqrt{\langle r_q^2 \rangle}$ and the size of the neutron skin is satisfactorily described within the extended Thomas-Fermi approximation. The sensitivity of the calculations of nuclear rms radii $\sqrt{\langle r^2 \rangle}$ to the choice of the force parametrization can be used to a fit of Skyrme forces. We have pointed that the charge radii of proton distributions show the shell oscillations with A which are related to the shell effects in the Coulomb energy. The charge radii are connected to the isospin shift of neutron-proton chemical potentials $\Delta\lambda = \lambda_n - \lambda_p$ for nuclei beyond the beta-stability line by fixed value of the mass number A [18]. It was shown that the isovector shift of the nuclear radius Δr_{np} is primarily linear dependent on the asymmetry parameter X. The Coulomb and spin-orbit interactions do not affect significantly the isovector shift of the nuclear radius.

We have established the influence of the polarization effect given by Eq. (25) on the rms radius $\sqrt{\langle r_n^2 \rangle}$ of the neutron distribution. This effect increases with the asymmetry parameter X and can be responsible for the appearance of the giant neutron halo in the nuclei close to the drip line. We have also estimated the relative contribution to the value of the isotopic shift of radii Δr_{np} obtained from both the skin effect and the halo effect. The halo effect gives usually a minor contribution to the shift Δr_{np} and it can be comparable with the skin effect near the drip line only.

---

[1] J. Meng, H. Toki, J.Y. Zeng, S.Q. Zhang and S.-G. Zhou, Phys. Rev. C **65**, 041302 (2002).

[2] S. Mizutori, J. Dobaczewski, G.A. Lalazissis, W. Nazarewicz and P.-G. Reinhard, Phys. Rev. C **61**, 044326 (2000).

[3] A. Trzcińska, J. Jastrzébsky, P. Lubiński, F. J. Hartmann, R. Schmidt, T. von Egidy, and B. Kłos, Phys. Rev. Lett. **87**, 082501 (2001).

[4] A. Krasznahorskay, H. Akimune, A.M. van den Berg, *et al.*, Nucl. Phys. **A731**, 224 (2004).

[5] M. Warda, X. Viñas, X. Roca-Maza and M. Centelles, Phys. Rev. C **81**, 054309 (2010).

[6] M. Centelles, X. Roca-Maza, X. Viñas and M. Warda, Phys. Rev. C **82**, 054314 (2010).

[7] N. Nikolov, N. Schunck, W. Nazarewicz, M. Bender and J. Pei, Phys. Rev. C **83**, 034305 (2011).

[8] M.K. Gaidarov, A.N. Antonov, P. Sarriguren, and E. Moya de Guerra, Phys. Rev. C **84**, 034316 (2011).

[9] P. Hohenberg and W. Kohn, Phys. Rev. **136**, B 864 (1964).

[10] D.A. Kirzhnitz, *Field Theoretical Methods in Many Body-Systems* (Pergamon, London, 1967).

[11] M. Brack, C. Guet and H.-B. Håkansson, Phys. Rep. **123**, 275 (1985).

[12] V.M. Kolomietz, *Local Density Approach for Atomic and Nuclear Physics* (Naukova Dumka, Kiev, 1990; in Russian).

[13] V.M. Kolomietz and A.I. Sanzhur, Eur. Phys. J. **A38**, 345 (2008).

[14] W.D. Myers and W.J. Swiatecki, Ann. Phys. (NY) **55**, 395 (1969).

[15] W.D. Myers and W.J. Swiatecki, Ann. Phys. (NY) **84**, 186 (1974).

[16] P. Möller, J.R. Nix, W.D. Myers and W.J. Swiatecki, At. Data Nucl. Data Tables **59**, 185 (1995).

[17] P. Danielewicz, Nucl. Phys. **A 727**, 233 (2003).

[18] V.M. Kolomietz, S.V. Lukyanov and A.I.Sanzhur, Nucl. Phys. At. Energy **11**, 335 (2010).

[19] K. Oyamatsu, I. Tanichata, S. Sugahara, K. Sumiyoshi and H. Toki, Nucl. Phys. **A 634**, 3 (1998).

[20] K. Oyamatsu and K. Iida, Progr. Theor. Phys. **109**, 631 (2003).

[21] B.A. Brown, Phys. Rev. Lett. **85**, 5296 (2000).

[22] S. Typel and B.A. Brown, Phys. Rev. C **64**, 027302 (2001).

[23] R.J. Furnstahl, Nucl. Phys. **A 706**, 85 (2002).

[24] V.M. Kolomietz and A.I. Sanzhur, Phys. Rev. C **81**, 024324 (2010).

[25] T. Suzuki, H. Geissel, O. Bochkarev, *et al.*, Phys. Rev. Lett. **75**, 3241 (1995).

[26] L. Ray, Phys. Rev. C **19** , 1855 (1979).

[27] V.E. Starodubsky, N.M. Hintz, Phys. Rev. C **49**, 2118 (1994).

[28] S. Karataglidis, K. Amos, B.A. Brown, P.K. Deb, Phys. Rev. C **65**, 044306 (2002).

[29] B.C. Clark, L.J. Kerr, S. Hama, Phys. Rev. C **67**, 054605 (2003).